

A differentiable binary microlensing model using adaptive contour integration method

HAIBIN REN (任海滨) ¹ AND WEI ZHU (祝伟) ¹

¹*Department of Astronomy, Tsinghua University, Beijing 100084, China*

ABSTRACT

We present `microlux`, which is a Jax-based code that can compute the binary microlensing light curve and its derivatives both efficiently and accurately. The key feature of `microlux` is the implementation of a modified version of the adaptive sampling algorithm that was originally proposed by V. Bozza to account for the finite-source effect most efficiently. The efficiency and accuracy of `microlux` have been verified across the relevant parameter space for binary microlensing. As a differentiable code, `microlux` makes it possible to apply gradient-based algorithms to the search and posterior estimation of the microlensing modeling. As an example, we use `microlux` to model a real microlensing event and infer the model posterior via both Fisher information matrix and Hamiltonian Monte Carlo, neither of which would have been possible without the access to accurate model gradients.

Keywords: Gravitational microlensing (672), Binary lens microlensing (2136), Algorithms (1883), Markov chain Monte Carlo (1889)

1. INTRODUCTION

Gravitational microlensing has been successful in detecting exoplanets and stellar binaries (Mao & Paczynski 1991; Gould & Loeb 1992). According to the NASA Exoplanet Archive (Akeson et al. 2013),¹ microlensing has discovered more than 200 planets, many of which have relatively wide orbits and/or low planet-to-star mass ratios. This makes microlensing one promising method for finding Earth-like exoplanets (e.g., Bennett & Rhie 1996; Penny et al. 2019) and complementing the other detection techniques in studying exoplanet demographics (e.g., Gaudi 2012; Zhu & Dong 2021).

The interpretation of planetary and binary-star microlensing (hereafter binary microlensing both together) events requires algorithms that can efficiently and accurately compute the microlensing light curve. When the source star is sufficiently away from the caustic curve, which is a set of points with infinite magnification, the source is effectively point-like and the microlensing magnification can be computed quite easily. However, when the source becomes close enough to the caustic, the finite size of the source cannot be

ignored, and the computation of the magnification involves a two-dimensional integration over the projected surface of the source. Several numerical algorithms have been made available to tackle this problem, including inverse ray shooting (Kayser et al. 1986), contour integral (Schramm & Kayser 1987; Gould & Gaucherel 1997; Dominik 1998; Bozza 2010), and hybrid algorithms that combine both (Dong et al. 2006; Dominik 2007). In particular, the contour integral method simplifies and accelerates the calculations by transforming the areal integral into one dimension via Green’s theorem. First introduced by Schramm & Kayser (1987), this method has been extensively used in binary microlensing (e.g., Gould & Gaucherel 1997; Dominik 1998, and thereafter).

One of the most widely used algorithms in computing the binary microlensing light curve is `VBinaryLensing` (Bozza 2010; Bozza et al. 2018).² By controlling several specifically designed error estimators, `VBinaryLensing` can perform adaptive sampling of the contour integration method and achieve smooth transition from the point-source approximation. This package has found extensive use in the modelings of many binary and planetary events (e.g., Zang et al. 2021) as well as several

Corresponding author: Wei Zhu
weizhu@tsinghua.edu.cn

¹ Based on a query made in December 2024.

² This package is now part of the new package `VBMicrolensing` (Bozza et al. 2024). The key functions related to binary microlensing remain unchanged.

open-source packages (e.g., [Poleski & Yee 2019](#); [Bachelet et al. 2017](#)).

With the diversified goals of microlensing studies as well as the upcoming new era of microlensing surveys, there is the need for new methods and frameworks in microlensing modeling. The existing surveys, most notably OGLE (Optical Gravitational Lensing Experiment, [Udalski 2003](#)), MOA (Microlensing Observations in Astrophysics, [Bond et al. 2001](#)), and KMTNet (Korea Microlensing Telescope Network, [Kim et al. 2016](#)), have altogether detected $> 10^5$ microlensing events, and the next generation of microlensing surveys are promised to detect even more events with higher quality ([Penny et al. 2019](#); [Yan & Zhu 2022](#)). Within these large datasets, events that are intrinsically rare occur, including those with dark lenses ([Sahu et al. 2022](#); [Lam et al. 2022](#); [Mróz et al. 2022](#)), lenses of multiple (≥ 3) components (e.g., [Gaudi et al. 2008](#); [Gould et al. 2014](#)), etc. While some clever search strategy can be adopted to identify some of those intrinsically rare but astrophysically interesting events, an improved modeling method and framework will almost certainly uncover more unexpected microlensing phenomena and allow us to study them in a more systematic way.

New tools on scientific programming have been made available especially driven by the advancement of the machine learning field. In particular, several modern packages have been developed that can automatically build the computational graph and apply the chain rule to obtain the model derivatives up to machine precision (i.e., automatic differentiation; e.g., [Julia](#), [Bezanson et al. 2017](#), [Jax](#), [Bradbury et al. 2018](#)). These modern packages use many new techniques that have improved the applicability and performance of the automatic differentiation method ([Margossian 2018](#)). There have been successful applications of this method in probabilistic programming (e.g., [Stan](#), [Carpenter et al. 2017](#)), machine learning (e.g., [PyTorch](#), [Ansel et al. 2024](#)), and many other fields. The modeling procedure of microlensing data may also be improved with the access to accurate model derivatives.

In this work, we introduce `microlux`, a `Jax`-based code for magnification and gradient calculations of binary microlensing. Compared to another similar attempt [Bartolić \(2023\)](#), our work focuses on the implementation of the adaptive sampling method of [Bozza \(2010\)](#) and can produce model gradients in an efficient and accurate manner. This paper is organized in the following way: Section 2 provides a brief overview of the adaptive sampling method and its implementation in `VBBinaryLensing`; Section 3 explains in details how the method is modified and implemented in `Jax`; Sec-

tion 4 provides tests that validate `microlux` and evaluate its performance; Section 5 demonstrates the utility of `microlux` by applying it to the analysis of a real, archival event; finally Section 6 provides a brief summary of the present work and short discussions about potential future applications and improvements.

2. OVERVIEW OF `VBBinaryLensing`

For any point on the source plane, its corresponding images can be obtained by solving the binary lens equation

$$\zeta = z - \frac{1/(1+q)}{\bar{z} - \bar{z}_1} - \frac{q/(1+q)}{\bar{z} - \bar{z}_2}. \quad (1)$$

Here $\zeta = y_1 + iy_2$ is the source position, q is the mass ratio, $z = x_1 + ix_2$ is the image position, \bar{z} is its complex conjugate, and \bar{z}_1 and \bar{z}_2 are the complex conjugates of the binary lens positions, respectively ([Witt 1990](#)). In `VBBinaryLensing`, the secondary lens is fixed at origin (i.e., $z_2 = 0$), and the primary lens is on the real axis at $-s$.

The binary lens equation (Equation 1) can be converted into a fifth-order complex polynomial and then solved numerically ([Witt 1990](#)). `VBBinaryLensing` applies the improved Laguerre method of [Skowron & Gould \(2012\)](#) and identifies all five solutions in an iterative way, which are later polished using the original polynomial to reduce the numerical error. Each solution has also an associated parity p , which is the sign of the determinant of the Jacobian ([Witt & Mao 1995](#))

$$\det J \equiv 1 - \left| \frac{\partial \zeta}{\partial \bar{z}} \right|^2. \quad (2)$$

The solutions are then substituted into the original lens equation to eliminate the spurious solutions. In doing so, `VBBinaryLensing` makes use of the known facts that (1) there are either three or five solutions of the binary lens equation, depending on whether the source is outside or inside the caustic, and (2) the sum of the parity of all true solutions should be -1 ([Witt & Mao 1995](#)). In addition, `VBBinaryLensing` also applies some empirical criteria related to the relative accuracy of the third and fourth worse solutions.

For a typical binary microlensing light curve, the point source approximation by summing up the inverse Jacobian determinant for each true image serves well for the majority of the time. To identify those source positions that require special treatment for the finite-source effect, `VBBinaryLensing` applies a number of tests to speed up the light curve calculation significantly ([Bozza et al. 2018](#)). At any source position where the point source approximation fails, `VBBinaryLensing` selects a sample

of points on the boundary of the source circle

$$\zeta = \zeta_c + \rho e^{i\theta_i}, \theta \in [0, 2\pi] \quad (3)$$

and solves the lens equation for their corresponding image positions. Here ζ_c is the position of the source center, ρ is the radius of the source normalized to the Einstein ring radius θ_E . In order to compute the total magnification, `VBBinaryLensing` computes the total area enclosed by the image points, using the numerical approximation of the Green's theorem

$$A_{\text{image}} = \sum_I p_I \sum_i (\Delta A_{I,i}^{(t)} + \Delta A_{I,i}^{(p)}). \quad (4)$$

Here p_I is the parity of the I -th image, $\Delta A_{I,i}^{(t)}$ is the trapezoidal approximation of the line integral from the argument interval $(\theta_i, \theta_i + \Delta\theta)$,

$$\Delta A_{I,i}^{(t)} = \frac{1}{2} \mathbf{x}_I(\theta_i) \wedge \mathbf{x}_I(\theta_i + \Delta\theta), \quad (5)$$

and $\Delta A_{I,i}^{(p)}$ is the parabolic correction

$$\Delta A_{I,i}^{(p)} = \frac{1}{24} [(\mathbf{x}'_I \wedge \mathbf{x}''_I)|_{\theta_i} + (\mathbf{x}'_I \wedge \mathbf{x}''_I)|_{\theta_i + \Delta\theta}] \Delta\theta^3. \quad (6)$$

The symbol $\mathbf{x}_I(\theta_i)$ denotes the I -th image position vector of the point on the source boundary with angle θ_i , and $\mathbf{x}'_I(\theta_i)$ is its derivative with respect to θ .

In the core of `VBBinaryLensing` is its strategy to adaptively sample points on the boundary of the source circle according to the requirement magnification precision (Bozza 2010). There are a few notable features in this adaptive sampling process. First, `VBBinaryLensing` starts with two points and every iteration adds one new sampling to the source arc that contributes largest to the magnification error. There is in principle no limit on the maximum number of sampling points. Second, once a new point is added, the corresponding image positions are connected to the closest points on the existing image polygons with the same parity. Third, the total error estimator, given first in Bozza (2010) and recently updated in Bozza et al. (2024), concerns only the estimated error on the microlensing magnification.

To deal with the limb darkening effect, `VBBinaryLensing` divide the source into several concentric annuli with different constant average brightness according to the limb darkening profile. The total magnification is the weighted sum of the uniform brightness magnification on these annuli. Similar to the adaptive sampling, `VBBinaryLensing` also use several error estimators to optimize the division until the total error reach the desired accuracy.

3. REALIZATION OF `microlux`

The implementation of the adaptive sampling algorithm in `Jax` is not a simple translation of `VBBinaryLensing` from `C++` into `Jax`. This is because `VBBinaryLensing` makes use of the flexible data structures such as the linked list and a number of dynamical algorithms in `C++`. As an array-oriented and vectorized programming language, `Jax` works the best with arrays with fixed shapes. Because of the differences between the two languages, a number of changes need to be made to realize the adaptive sampling method, as will be detailed later in this section. The advantage of using `Jax` is of course the automatic differentiation, and we show in Section 3.5 how it is achieved.

3.1. Solving Lens Equation

As mentioned in Bozza (2010), most of the computing time in `VBBinaryLensing` is spent in solving the lens equation, so it is crucial to adapt a suitable root-finding algorithm. `VBBinaryLensing` uses the Skowron & Gould (2012) algorithm, which identifies solutions successively. In order to achieve high performance in `Jax`, the lens equation solver should be parallelized and vectorized. This calls for an algorithm that can identify all roots of the polynomial equation simultaneously.

We adopt the Aberth–Ehrlich method (Aberth 1973; Ehrlich 1967), which uses an implicit deflation strategy and can solve all the roots of polynomials simultaneously (see also Bartolić 2023). The update formula is given by

$$z_k^{\text{new}} = z_k - \left(\frac{P'(z_k)}{P(z_k)} - \sum_{j=1, j \neq k}^n (z_k - z_j)^{-1} \right)^{-1}. \quad (7)$$

Here $P(z_k)$ and $P'(z_k)$ are the function value and the derivative of the polynomial with order n evaluated at z_k , respectively, with z_k the k -th root. The above update rule is similar to that of the standard Newton's method, except for the addition of the second term in the denominator. As long as the initial guesses are not off by a significant amount, the convergence of the Aberth–Ehrlich method is cubic (Aberth 1973; Ehrlich 1967), similar to the Laguerre method that is commonly used for polynomial root findings. We use the method proposed by Fatheddin & Sajadian (2022) to set the initial guess for the first point, and use the roots from the previous polynomial as the initial guess for the next, in order to achieve better performance.

To identify the real roots and get the correct parity, we make use of the two physical properties in the binary lens case and a relative tolerance criterion once the solutions are inserted back into the original lens equation in the same way as `VBBinaryLensing` (see Section 2).

3.2. Connecting Image Contours

Once the image positions are obtained, the task is then to connect these points into image contours. For regular cases, the basic rule is to connect two image points with the minimum distance and the same parity. When there are image creations (i.e., caustic entrance, with image number changing from three to five) or image destructions (i.e., caustic exit, with image number changing from five to three), there are extra points for certain source positions that need to be connected to each other.

We use the Jonker–Volgenant algorithm (Jonker & Volgenant 1987) to solve the linear sum assignment problem and connect all the image points. The cost matrix that includes both the geometric distance and the parity information is given by

$$C_{m,n,i} = |z_{i-1}[m] - z_i[n]| + K|p_{i-1}[m] - p_i[n]|, \quad (8)$$

where $C_{m,n,i}$ is the cost between the m -th image of the source position with θ_{i-1} , $z_{i-1}[m]$, and the n -th image of the next source position with θ_i , $z_i[n]$, and $p_{i-1}[m]$ and $p_i[n]$ are the corresponding parity values, respectively. The parameter K is a tunable constant to ensure the image match with same parity, and we find $K = 5$ is a reasonable number. The cost matrix will be a square matrix of shape (5, 5) or a rectangular matrix of shape either (5, 3) (for image destruction) or (3, 5) (for image creation). The latter cases are also called unbalanced assignments.

We implement the modified Jonker–Volgenant algorithm, which can handle the unbalanced assignments and is currently used in `scipy.optimize.linear_sum_assignment` (Crouse 2016), in `Jax`. This algorithm is guaranteed to find the global best match and thus robust, making it suitable for the problem of imaging connecting in our code. Although the theoretical time complexity of the Jonker–Volgenant algorithm is $O(n^3)$, the actual executing time is short because the matching between the majority of the points is already satisfied when we use the roots from last θ sampling as the initial guess (see Section 3.1). Given these properties, we suggest that people consider this method in connecting the image contours in the triple-lens (and potentially higher multiples) case.

3.3. Adaptive Sampling

Adding the sampling points one-by-one is very inefficient to fulfill optimal performance in `Jax` because of the frequent data movement. Given that the optimal sampling requires eight points at least (Bozza et al. 2018), we choose to start with more points (30 by default, see Section 4) and add multiple points in multiple intervals

in a single iteration. Within each θ interval, the number of points to be added within the interval (θ_i, θ_{i+1}) is determined by

$$N_{\text{new},i} = \min\left(\left[\left(\frac{E_i\sqrt{N}}{k\epsilon}\right)^{\frac{1}{5}}\right], N_{\text{max}}\right). \quad (9)$$

Here E_i is the value of the error estimator in the certain θ interval (θ_i to θ_{i+1}), N is the current total number of points in this iteration, ϵ is the accuracy goal for the magnification calculation, k is a parameter that is empirically chosen to transform the accuracy goal of total magnification into the accuracy in the given θ interval and is set to $k = 2$ by default, and $N_{\text{max}} = 4$ is also an empirical upper limit to avoid over-sampling when the error estimators explode. The above formula is derived from the relative difference between the tolerance (ϵ) and the current error (E_i), and the power law index chosen here is the order of the error estimator. With the above sampling strategy, we can then use vectorization to improve the performance of the code.

Similar to `VBBinaryLensing` (Bozza et al. 2018), we also include the quadrupole test (Pejcha & Heyrovský 2009; Gould 2008; Cassan 2017), ghost image test, and planetary test to identify the regions where the special treatment for the finite-source effect is needed.³

To account for the limb-darkening effect, we also use the weighted sum of magnifications from a number of concentric annuli, each with uniform surface brightness and contributing equally to the total source area. In its current implementation, `microlux` follows the general convention and adopts the linear limb-darkening law (Milne 1921). The number of concentric annuli is set to 10 by default, which is sufficient for the general purpose (e.g., Dong et al. 2006), although this number can be easily modified by the user.

3.4. Using Arrays with Fixed Lengths

`Jax` provides users a `numpy`-like interface with a `C`-like execution performance via the Just-In-Time (JIT) compilation (Bradbury et al. 2018). However, to make use of JIT compilation, users are required to fix the shapes of arrays in the code, which is not naturally achieved in dynamical problems such as the adaptive sampling of microlensing.

Here we use a dynamic array-like structure and pre-define multiple arrays of fixed and increasing lengths.

³ Note that there is inconsistency between some of the equations related to these tests in Bozza et al. (2018) and their realizations in `VBBinaryLensing` (V. Bozza, private communication). These have been corrected in `microlux`.

Whenever contour integration is invoked, we start with the array of the shortest length, which is set to 30 by default but adjustable by the user. This is sufficient to cover most cases that need the contour integral method (see Section 4.1). At each iteration of the adaptive sampling, we examine the total number of points against the length of the current array. If the current array is long enough, then the newly added points are assigned to the current array. Otherwise, all elements in the array are copied to the array of a longer length to avoid overflow. This data movement continues during the iterations of adaptive sampling, until the stopping criterion of the adaptive sampling is met or the total number of sampling points exceeds the maximum length (480 by default) of all arrays. In this latter situation, which is rarely encountered with our choices of the array lengths (see Section 4), the adaptive sampling stops and a warning is issued. The magnification in the last iteration is chosen as the final result.

Our above approach requires more memory and comes with longer JIT compilation time, but the price is affordable in order to enable fast execution and automatic differentiation.

3.5. Automatic Differentiation

Once the code is written in `Jax`, it is generally straightforward to obtain automatic differentiation via functions like `jax.jacfwd` or `jax.jacrev`. However, it is not guaranteed that these functions will always produce the correct results. There are a few features in `microlux` that require special treatments in order to have the automatic differentiation work properly.

First, for iterative algorithms like root-finding, the numerical instability may lead to `NaN` values in the returned derivatives. To avoid such a situation, we use the implicit function theorem to get the derivatives of the roots with respect to the polynomial coefficients. Specifically, for a polynomial of order n

$$f(a_k, z) = \sum_{k=0}^n a_k z^k, \quad (10)$$

where $\{a_k\}$ are the coefficients and z the variable of the polynomial, the derivatives of one given root $z = z_0$ with respect to the polynomial coefficients are given as

$$\frac{\partial z_0}{\partial a_k} = \left[-\frac{\partial f}{\partial a_k} / \frac{\partial f}{\partial z} \right] \Big|_{z=z_0}. \quad (11)$$

This conversion can be achieved via `Jax.lax.custom_root`. With this modification, the computational graph in automatic differentiation is also simplified.

Second, for iterative algorithms like adaptive sampling, there is no need to trace the gradients inside all

loops, and analytical results are available to accelerate the calculations and reduce the memory cost. We therefore stop the gradient tracing at the function that performs the adaptive sampling and use `Jax.custom_jvp` to set up a custom JVP (Jacobian-vector product) rule. Following Bozza (2010), the derivative of a source position ζ with respect to any model parameter Θ can be derived from Equation (1) ⁴

$$\frac{\partial \zeta}{\partial \Theta} = \frac{\partial z}{\partial \Theta} + \frac{\partial \zeta}{\partial \bar{z}} \frac{\partial \bar{z}}{\partial \Theta} + \frac{\partial q}{\partial \Theta} \frac{\partial \zeta}{\partial q} + \frac{\partial s}{\partial \Theta} \frac{\partial \zeta}{\partial s}, \quad (12)$$

where

$$\frac{\partial \zeta}{\partial \bar{z}} = \frac{1}{1+q} \left[\frac{1}{(\bar{z}-s)^2} + \frac{q}{\bar{z}^2} \right], \quad (13)$$

$$\frac{\partial \zeta}{\partial q} = \frac{1}{(1+q)^2} \left(\frac{1}{\bar{z}-s} - \frac{1}{\bar{z}} \right), \quad (14)$$

and

$$\frac{\partial \zeta}{\partial s} = -\frac{1}{1+q} \frac{1}{(\bar{z}-s)^2}. \quad (15)$$

Together with its complex conjugate, Equation (12) yields

$$\frac{\partial z}{\partial \Theta} = \left[\frac{\partial \zeta}{\partial \Theta} - \frac{\partial \zeta}{\partial \bar{z}} \frac{\partial \bar{z}}{\partial \Theta} - \frac{\partial q}{\partial \Theta} \left(\frac{\partial \zeta}{\partial q} - \frac{\partial \bar{\zeta}}{\partial \bar{q}} \frac{\partial \bar{\zeta}}{\partial \bar{z}} \right) - \frac{\partial s}{\partial \Theta} \left(\frac{\partial \zeta}{\partial s} - \frac{\partial \bar{\zeta}}{\partial \bar{s}} \frac{\partial \bar{\zeta}}{\partial \bar{z}} \right) \right] J^{-1}. \quad (16)$$

With this custom JVP rule we can also achieve reverse mode automatic differentiation in the `while` loops, which otherwise is not achievable in `Jax` ⁵.

Another issue is related to the adaptive step size in the numerical integration (Eberhard & Bischof 1999). Because the step size is adjusted based on the model parameters, it is also an implicit function of the model parameters. Directly applying the chain rule to the numerical integration with the parabolic correction, one would have

$$\frac{\partial (\Delta A_{I,i}^{(p)})}{\partial \Theta} = \frac{\partial f(\mathbf{x})}{\partial \Theta} \Delta \theta^3 + f(\mathbf{x}) \frac{\partial (\Delta \theta^3)}{\partial \Theta}, \quad (17)$$

where $f(\mathbf{x}) \equiv [(\mathbf{x}'_I \wedge \mathbf{x}''_I)|_{\theta_i} + (\mathbf{x}'_I \wedge \mathbf{x}''_I)|_{\theta_i + \Delta \theta}] / 24$ (Equation 6). While the second term on the right hand side of Equation (17) is introduced by the code, only the first term is needed for the correct derivatives. To resolve the issue, we use `Jax.lax.stop_gradient` to stop the gradient trace of the step size in the automatic differentiation.

⁴ The following derivations assume the primary lens at s .

⁵ https://jax.readthedocs.io/en/latest/_autosummary/jax.lax.while_loop.html

Finally, the convergence of the function value in the adaptive sampling does not necessarily lead to the convergence of the derivatives. This is especially true in binary lensing because of the existence of singularity at caustic. The experiment that will be shown in Section 4.2 indicates that the derivatives of the numerical integration to the binary microlensing parameters become so large that the original error estimators do not promise the convergence of the model derivatives. To solve this problem, we introduce a new error estimator

$$E_{I,i}^d = \frac{1}{240} |(\mathbf{x}'_I \wedge \mathbf{x}''')_{\theta_i} - (\mathbf{x}'_I \wedge \mathbf{x}''')_{\theta_{i+1}}| \Delta\theta^3. \quad (18)$$

Here $\mathbf{x}'_I \wedge \mathbf{x}'''$ can be obtained from the analytical formula

$$\mathbf{x}' \wedge \mathbf{x}''' = \frac{\partial \text{Im} \left[(z')^2 \zeta' \frac{\partial^2 \bar{\zeta}}{\partial z^2} \mathbf{J}^{-1} \right]}{\partial \theta}. \quad (19)$$

Similar to the first error estimator of `VBinaryLensing` (Bozza 2010), this new error estimator will add more sampling points where the derivatives of the numerical integration (especially the parabolic correction item) are large. Because the original error estimators are enough to ensure dense sampling around critical points and the calculations of these third derivatives are heavy, the new error estimator is only added in the ordinary images at caustic crossing.

4. CODE VALIDATION & PERFORMANCE

We use `VBinaryLensing` (version = 3.6.2) as the benchmark to show the robustness and speed of `microlux` in magnification calculations. The gradient results of `microlux` are compared against the numerical gradients of `VBinaryLensing`, which, as will be shown later, do not necessarily produce the correct results. A more robust validation of the gradient calculation is given in Section 5, in which `microlux` is applied to the analysis of a real light curve.

4.1. Microlensing Magnification

To validate the magnification results of `microlux` against `VBinaryLensing`, we first generate 1000 combinations of binary lens parameters, with $\log q$, $\log s$, and $\log \rho$ randomly drawn from $(-6, 0)$, $(-0.5, 0.5)$, and $(-3, -1)$, respectively. For each parameter combination, we then use both `microlux` and `VBinaryLensing` to generate magnification maps with the dimensions of 1000×1000 in the range $-4 < x < 3$ and $0 < y < 2$. In these calculations, we have set the relative tolerance (i.e., $\Delta A/A$) to 10^{-3} for `microlux` and 10^{-4} for `VBinaryLensing`, which is used as the ground truth. We also increase the maximum length of the array related to adaptive sampling (Section 3.4) to 960 to avoid

overflow. One of the randomly generated magnification maps is shown in the left panel of Figure 1, and the deviations relative to the similar map produced by `VBinaryLensing` are shown in the right panel. The maximum deviation remains below the chosen tolerance, suggesting that the two codes produce very similar results at least in this particular example.

Out of 10^9 grid points, about 8×10^7 fail the quadrupole test and thus require contour integration. This subset of grid points are used to investigate the computational efficiency and accuracy of our code. With our choice of the sampling strategy, the uniform sampling with 30 initial points is enough to meet the precision requirement for $\sim 86.7\%$ of the cases, whenever the contour integration is invoked. For the remaining $\sim 13.3\%$ of cases, additional samplings should be added via the adaptive sampling strategy in order to meet the precision requirement. The final number of sampling points are shown in Figure 2 as a function of the microlensing magnification. Higher magnifications generally require more sampling points, although at any given magnification the exact number can vary substantially. Within the parameter space that is tested here, the maximum magnification is around 1000, and the maximum number of points needed is around 400, much below the maximum length size (960) used in these calculations.

The fractional difference in magnification is shown in Figure 3 as a function of the magnification for all the grid points that require contour integration. All except for 50 of the $\sim 8 \times 10^7$ grid points are below the precision tolerance of 10^{-3} , indicating an overall good agreement between the two codes. Of the 50 grid points that exceed the precision tolerance, the majority (49/50) are still close to (i.e., below two times, indicated by the blue dashed line in Figure 3) the tolerance and considered acceptable.⁶ For the single grid point that exceeds twice the precision tolerance, the lensing geometry is shown in Figure 4, and the relatively large deviation comes from the under-sampled cusp region. As the deviation is still small, we do not further modify the code to account for such a rare case. Situations like this one, which have extremely large sources encountering tiny caustics, are also intrinsically rare in the analysis of realistic binary microlensing events.

Regarding the computational speed, `microlux` is 1.5–5 times slower than `VBinaryLensing` in generating magnification maps with the same microlensing param-

⁶ The error estimators contain a few parameters that are empirically determined. One can in principle choose to modify them to improve the precision, but we consider it unnecessary given that the difference remains small and acceptable.

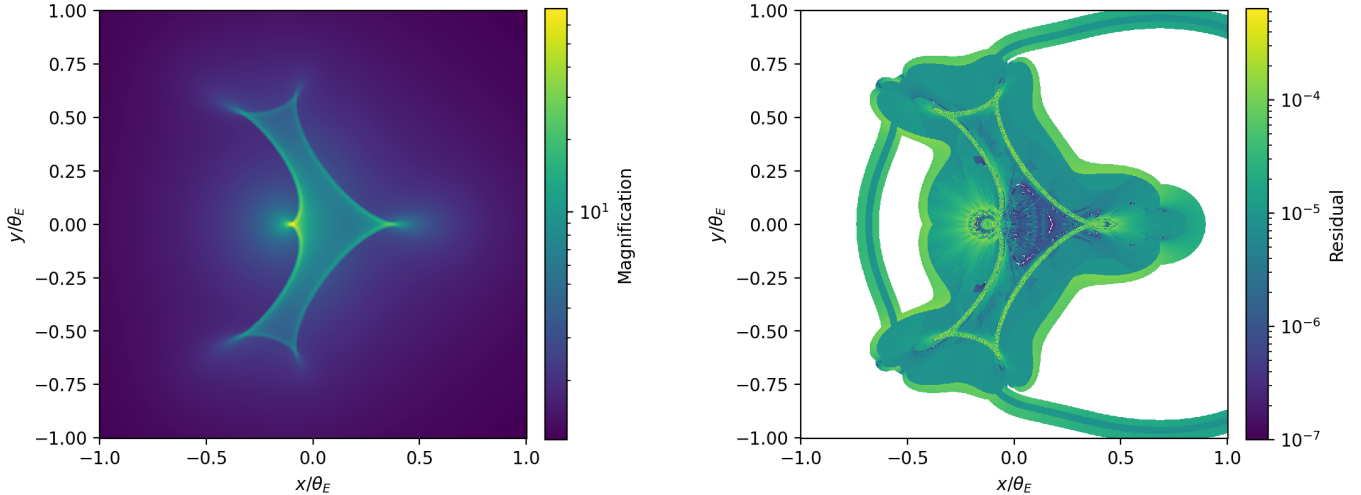


Figure 1. The left panel shows the magnification map produced by `microlux` for a binary lens configuration with $s = 0.9$, $q = 0.2$, and $\rho = 10^{-3}$, and the right panel is the fractional deviation in magnification between `microlux` and `VBinaryLensing`. In both calculations, we have set both the absolute tolerance and the relative tolerance to 10^{-3} . The two codes produce very similar magnification maps, and the small deviations arise from the regions where the quadrupole test fails, either in `VBinaryLensing` or `microlux` or both, and thus the finite-source effect with adaptive sampling is required. The largest deviation in this magnification map is 4.6×10^{-4} . Deviations below 10^{-7} are shown in white.

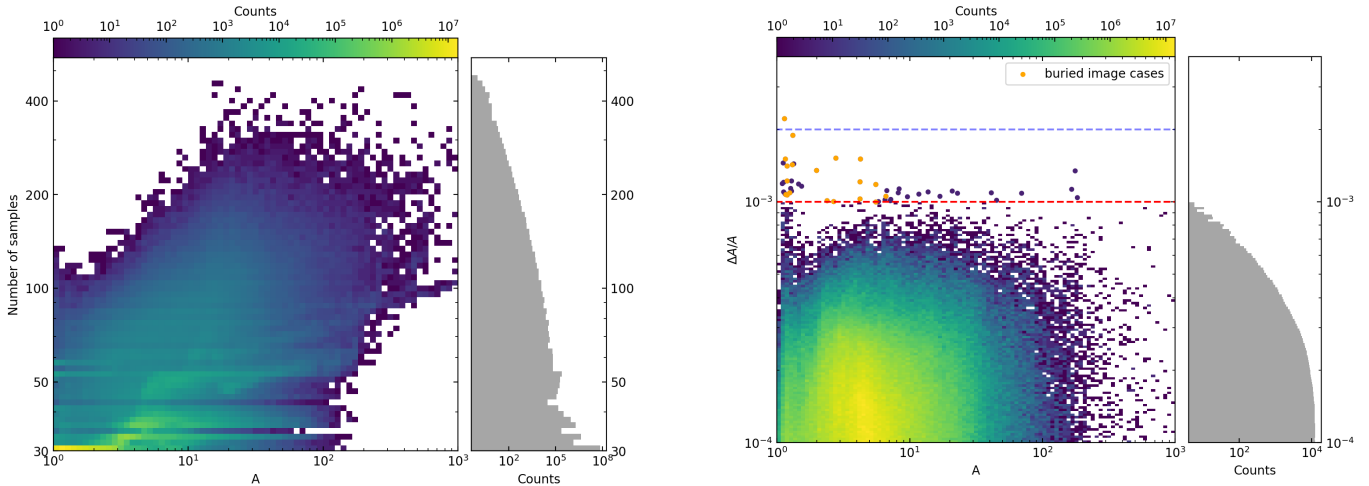


Figure 2. The left panel shows the total number of sample points used in the contour integration as the function of the microlensing magnification, color-coded by the number counts. The right panel shows the histogram distribution of the sampling points.

eters and precision requirement. The exact slow-down factor depends on the fraction of grid points that fail the point source approximation and thus require contour integrals. For example, the computing time of the magnification map shown in Figure 1 is 22s for `VBinaryLensing`, whereas it is 69s, thus a factor of 3 longer for `microlux` for the same parameter setting. The above tests are done on a M2 MacBook pro with `Jax` version = 0.4.29. As the primary goal of `microlux`

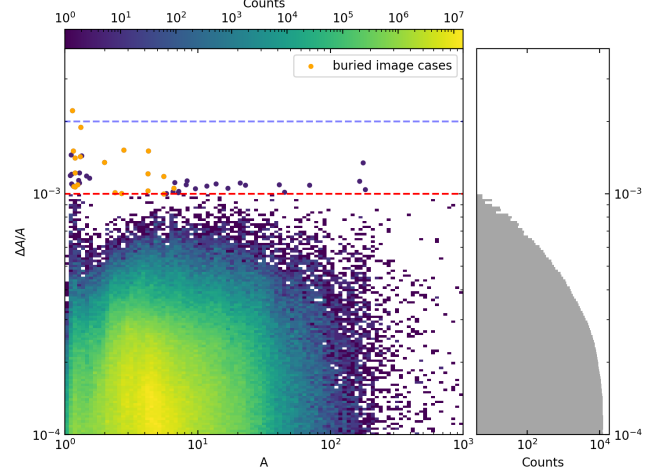


Figure 3. The left panel shows the fractional difference in microlensing magnification between `VBinaryLensing` and `microlux`, color-coded by the number counts. The red and blue dashed horizontal lines indicate the precision tolerance used in this test and twice of it, respectively. Of the $\sim 8 \times 10^7$ grid points shown here, 50 are above the red dashed line, the majority of which remain very close to the precision requirement. The maximum difference reaches 2.22×10^{-3} , due to the hidden cusp (see Figure 4). All cases (19 in total) that failed to reach the precision requirement due to the same reason are marked in orange.

is to provide accurate model gradients rather than to compete with `VBinaryLensing` in the computation efficiency of microlensing magnifications, the speed difference of a factor of a few is sufficient for our pur-

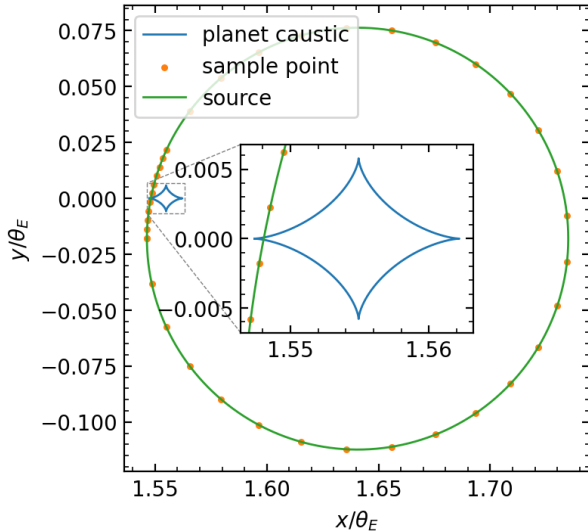


Figure 4. This figure shows the source star (green) and the caustic curve (blue) that correspond to the grid point in Figure 3 with the largest deviation in microlensing magnification between `microlux` and `VBinaryLensing`. The key binary lens parameters are $\rho = 9.43 \times 10^{-2}$, $s = 2.04$, and $q = 1.81 \times 10^{-4}$. The orange dots are the sampled points according to the strategy of `microlux`. The inset plot shows a zoom-in view around the intersection between the giant source and the tiny caustic. The cusp to the left is under sampled (i.e., a hidden cusp), which results in a relatively large deviation of 2.22×10^{-3} in the microlensing magnification. Such extreme cases are rarely encountered in realistic microlensing events.

pose. Nevertheless, we identify the primary causes of the speed difference as: (1) the less optimal sampling strategy (Section 3.3) and (2) the less efficient polynomial solver (Section 3.1). Both have been chosen to increase the computational performance in `Jax`. Additionally, the use of arrays with fixed lengths (Section 3.4) and the less efficient data movement in arrays compared to linked lists also contribute to the speed difference. Some of these issues are the subjects of future optimization of our code.

4.2. Gradient

We use `jax.jacfwd` to obtain the model gradients. An example is given in Figure 5, which shows the microlensing light curve and its partial derivative with respect to the source scaled size ρ . The automatic differentiation of `microlux` with the addition of the new error estimator E^d (Equation 18) gives a smooth curve for the chosen gradient. For comparisons, the result of `microlux` without E^d and the gradient calculated by `VBinaryLensing` based on finite difference both produce erroneous gradient curves, evidenced by the numerous spikes during the caustic crossing regions. In calculating the gradient

with `VBinaryLensing` via the finite difference method, we have used `scipy.approx_fprime` with the default step size ($\delta\rho \approx 1.5 \times 10^{-8}$) and set the precision tolerance to $\Delta A/A = 10^{-3}$. The accuracy in the gradient can in principle be improved with a much lower tolerance, but that would substantially reduce the speed of `VBinaryLensing` with no guarantee on the accuracy of the gradient. For completeness, we show the derivatives of the same light curve model with respect to the other model parameters in Figure 6.

Our code provides accurate model gradients in a computationally efficient way. The computational time of the seven gradients and the magnification value altogether is only 2–3 times longer than the computational time of the magnification value alone.⁷ For comparisons, the finite difference method will need eight function evaluations to obtain the gradients of seven parameters, in addition to its incapability to yield accurate gradients.

5. APPLICATION TO A REAL EVENT

Access to accurate model gradients allows us to use gradient-based methods in the search for best-fit model parameters and the estimation of the parameter posteriors. Here we demonstrate the application of `microlux` to the second task while leave the former to some future work.

We select the microlensing event KMT-2019-BLG-0371 as the example to demonstrate the utility of gradients in microlensing analysis and the robustness of our code. KMT-2019-BLG-0371 is a relatively short-timescale ($t_E = 6.65$) binary-lens event with $q = 7.24 \times 10^{-2}$ and prominent caustic-crossing features (Kim et al. 2021). This event has degenerate solutions, but here we only focus on the small s solution. We assume that the best-fit parameters have been identified and focus on the estimation of the parameter posteriors.

Besides the seven parameters that are needed to describe the microlensing magnification $A(t)$ at a given time t , two flux parameters for each data set are usually needed to model the actual microlensing light curve

$$F(t) = F_S \cdot A(t) + F_B. \quad (20)$$

Here F_S is the flux of the source star in the absence of lensing, and F_B is the blending flux. For simplicity, below we use the aligned light curve and thus only one set of F_S and F_B is needed. As Equation (20) is linear, the derivatives of the model flux with respect to all model parameters (i.e., the seven magnification parame-

⁷ For the specific example shown in Figures 5 and 6, they are 4.09s and 1.47s, respectively.

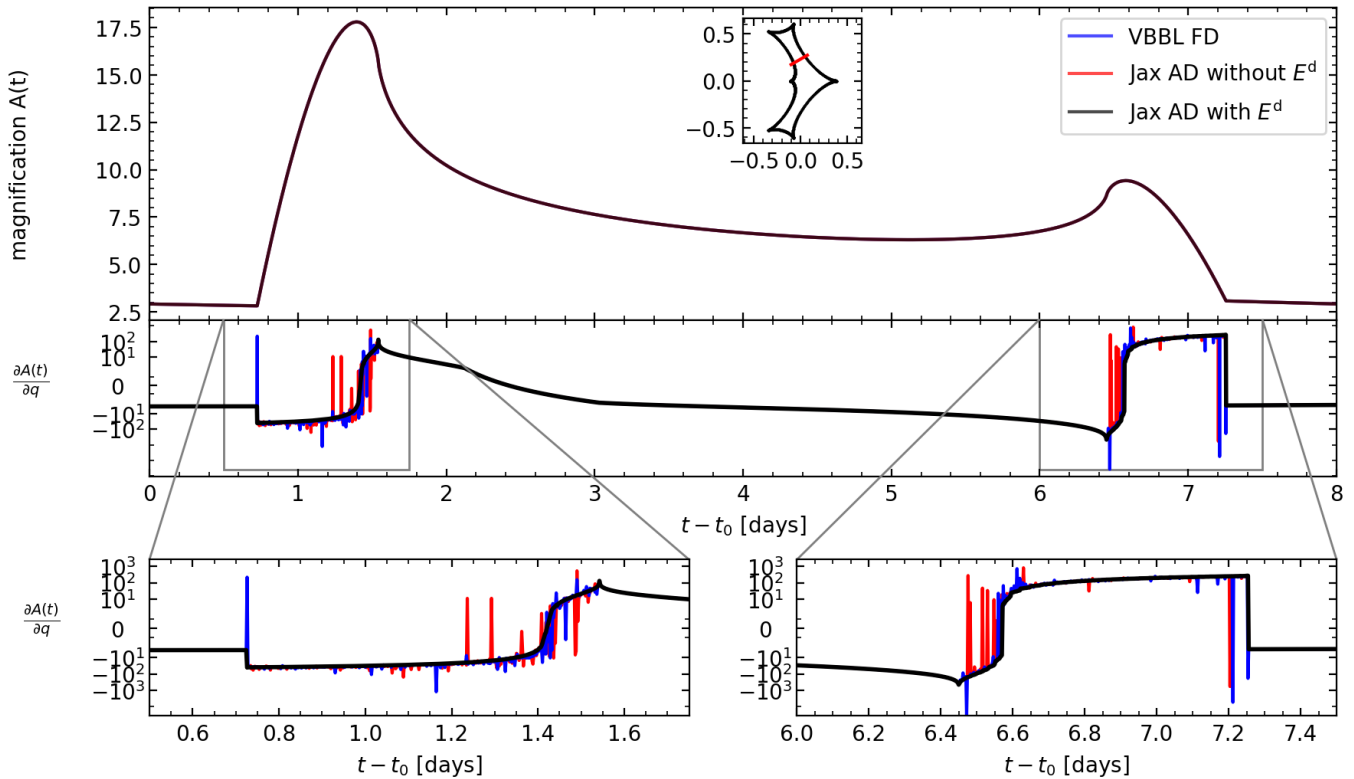


Figure 5. An example binary-lens light curve (top panel) and its derivative with respect to the planet-to-star mass ratio q (middle panel). Three different methods have been used here, including using `microlux` with (black curve) and without (red curve) the new error estimator term, E^d , and using `VBBinaryLensing` through the finite difference method (blue curve; implemented in `scipy.approx_fprime`). The bottom panels show the zoom-in views of the two caustic crossing regions. The inset in the top panel illustrates the binary-lens geometry (caustic and trajectory), with $q = 0.2$, $s = 0.9$, and $\rho = 10^{-2}$. Only `microlux` with E^d is able to yield smooth (and accurate) model gradient curve.

ters and the two flux parameters) can be easily derived, given the gradients of $A(t)$ from `microlux`.

5.1. Fisher Information Matrix

For binary lens events, the model posterior can often be described as a multivariate Gaussian. Once the best-fit parameters are known, the covariance matrix of the Gaussian is given by the inverse of the Fisher information matrix, which is defined as

$$\mathcal{F}_{ij} = \sum_k \frac{1}{\sigma_k^2} \frac{\partial F(t_k)}{\partial \Theta_i} \frac{\partial F(t_k)}{\partial \Theta_j}. \quad (21)$$

Here Θ_i is the i -th model parameter, and $F(t_k)$ and σ_k are the model light curve and the observed flux uncertainty at epoch t_k , respectively. In Figure 7, we compare the covariance matrix derived from the Fisher information matrix and that from the sampling method (see Section 5.2), and the agreement is excellent. It takes only one function evaluation to obtain the covariance matrix via the Fisher information approach.

The model posterior may deviate, sometimes substantially, from a multivariate Gaussian. This usually hap-

pens when the correlations between certain model parameters are strong and/or the constraints on certain parameters are weak. In the first case, a multivariate Gaussian can still be achieved and the Fisher information approach remains applicable as long as the model can be reparameterized in a proper way (e.g., Zhu et al. 2015). In the latter situation, the Fisher information approach is still useful in estimating the covariances of those well-constrained parameters. It also serves as a useful starting point for the sampling approach to map the posterior in a more efficient way (see Section 5.2).

5.2. Hamiltonian Monte Carlo

Monte Carlo sampling methods are often used to map the model posterior. The access to model gradient of `microlux` allows us to employ more efficient Monte Carlo methods other than the commonly used standard Markov Chain Monte Carlo (MCMC, e.g., Foreman-Mackey et al. 2013).

Here we use Hamiltonian Monte Carlo (HMC, Duane et al. 1987; Neal 2011) to showcase the potential of `microlux` in efficiently sampling the posterior distri-

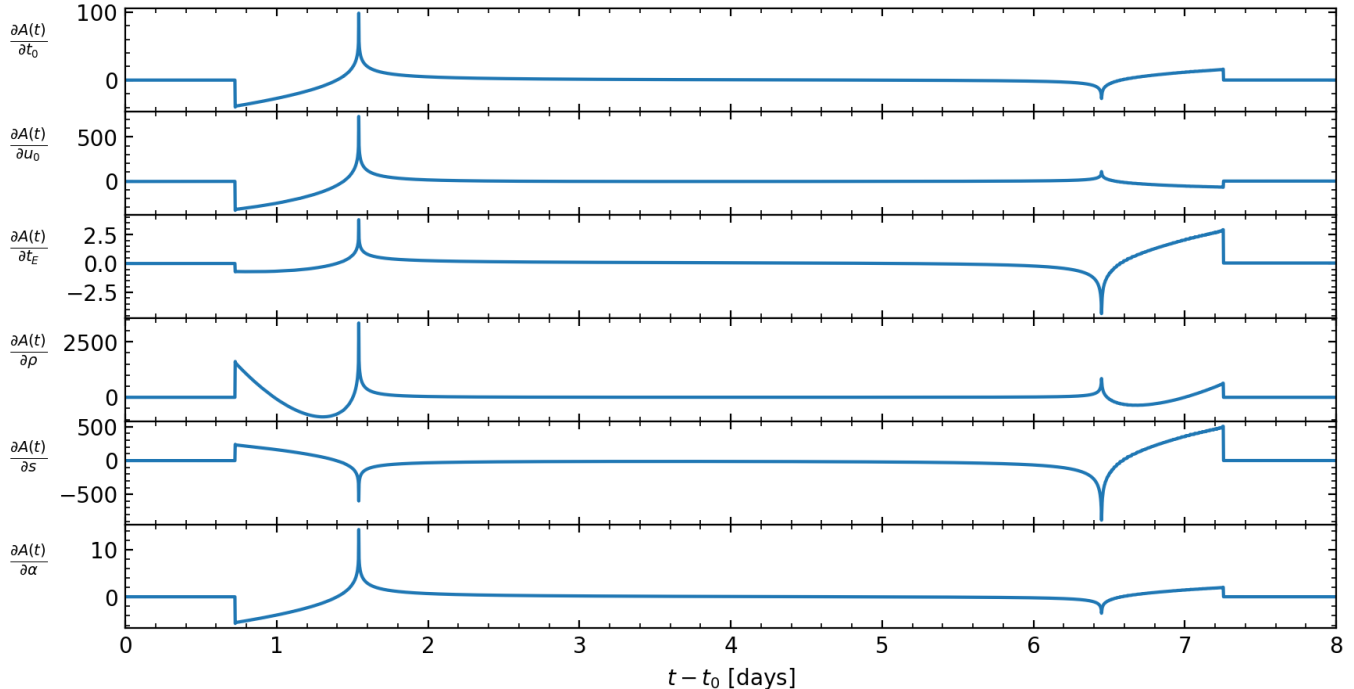


Figure 6. Derivatives of the same binary light curve as in Figure 5 respect to the other microlensing parameters, obtained by `microlux` with the E_4 term.

bution. Specifically, we choose the No U-Turn Sampler (NUTS, Hoffman & Gelman 2011) in `Numpyro` (Bingham et al. 2019; Phan et al. 2019). To achieve better performances, we use the covariance matrix obtained from the Fisher information matrix approach (Section 5.1) to reparameterize the binary microlensing parameters, which largely removes the correlations between parameters and thus improves the efficiency in the warm-up stage in NUTS. We run 4 chains, each with 500 warm-up steps and 1000 sampling steps. The sampler works successfully with an average acceptance rate of 0.88. The resulting posterior distribution is also shown in Figure 7.

To fairly compare the performance of different samplers, we use Effective Sample Size (ESS) as the criterion (Geyer 2011). For the same dataset and initial condition, we obtain an ESS of 504 when using `emcee` with 40 chains and 2000 samples in each chain, yielding 158 function calls per ESS. For comparisons, NUTS combined with `microlux` obtains an ESS of 1726 based on 56712 function calls, thus about 33 function calls per ESS. Therefore, NUTS is more efficient than `emcee` by a factor of about five in this specific example.⁸ The difference in sampling efficiency is expected to be even larger

⁸ In terms of the speed, the difference in this case is also about five, with NUTS being faster. This is because the parallelization in `Jax` is more efficient than that in `emcee`, even though `microlux` is slower than `VBinaryLens` by a factor of a few.

once the posterior distribution becomes more complicated and/or the higher-order effects such as microlensing parallax and lens orbital motion are included. We leave a more detailed investigation of this to a future work.

6. DISCUSSION

We present `microlux`,⁹ which implements a modified version of the adaptive contour integration method of Bozza (2010) in the `Jax` library. This differentiable code can achieve efficient and accurate calculations of binary microlensing light curve and its gradient. Compared to the existing codes, a few notable differences are introduced in order to optimize the performance of `microlux` in `Jax`. These include the different algorithms to solve the lens equation and connecting the images, a different sampling strategy, and the use of dynamic data structures.

`microlux` is also specially designed to obtain accurate model gradients. In particular, we have introduced a new error estimator into the adaptive sampling algorithm in order to ensure the convergence of the gradient. We have tested the efficiency and accuracy of `microlux` against the existing code in the relevant parameter space of binary microlensing modeling. In its current imple-

⁹ <https://github.com/CoastEgo/microlux>

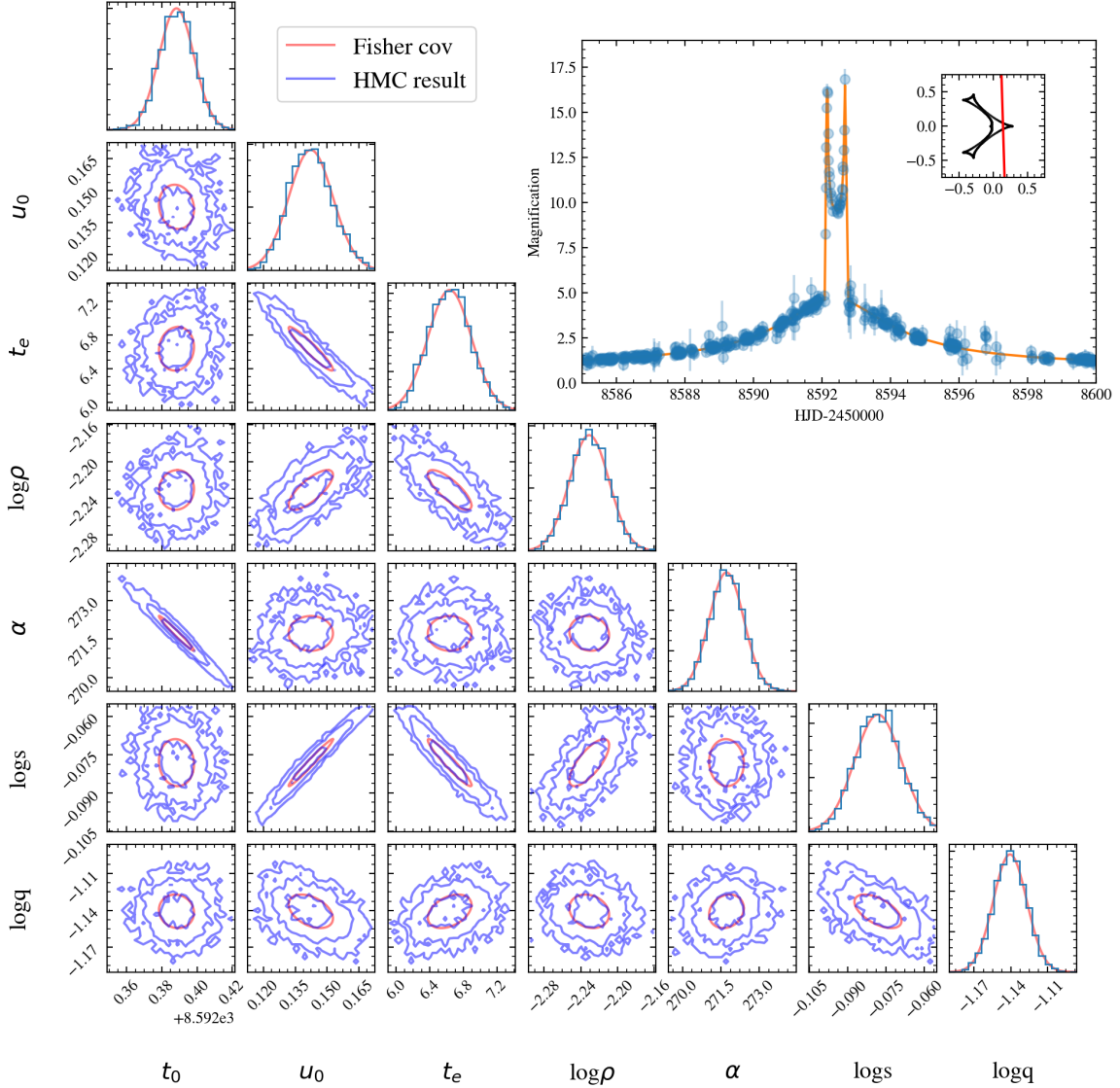


Figure 7. The corner plot illustrating the covariance matrices of KMT-2019-BLG-0371 from the Fisher information matrix approach (red curve) and the HMC sampling (blue curve). Only the $1\text{-}\sigma$ contours are shown in the former case, whereas the $1\text{-}3\sigma$ contours are shown in the HMC case. The light curve and the binary-lens geometry for the close solution are shown in the upper right figure.

mentation, `microlux` is slower by a factor of < 5 in computing the microlensing magnification, but can provide faster and more accurate evaluation of the model gradients.

The access to accurate model gradients can potentially speed up the modeling process of binary microlensing events. In Section 5, we have applied `microlux` to a real binary microlensing event to showcase its power in estimating the model posterior. Once the best-fit solution is known,¹⁰ the posterior distribution can be ob-

tained via the inversion of the Fisher information matrix, which only requires one function evaluation, or the advanced sampling method that utilizes the model gradients (e.g., HMC), which can achieve faster convergence than the standard MCMC approach. In addition, the differentiable nature of `microlux` may also improve the performance of machine learning models in predicting the parameters as well as their posteriors of binary microlensing events (Zhang et al. 2021; Zhao & Zhu 2022).

Finally, it is worth pointing out that there is still room for further optimization in `microlux`. As noted in Section 4.1, the sampling strategy and the polynomial solver are most responsible for the speed difference between `microlux` and `VBinaryLensing`. In the cur-

¹⁰ Although not demonstrated here, the search for the best-fit solution also benefits from access to the model gradients.

rent implementation, these two steps have been designed to balance the robustness and efficiency across the wide range of parameter space relevant for binary microlensing, they can certainly be further optimized if specific parameter ranges are concerned. For example, the semi-analytical root solver proposed by Zhang (2023) may perform better for typical planetary microlensing events. A more efficient use of the dynamical array and the implementation into GPU (Wang et al. 2025) may potentially speed up the code as well. We leave the investigation of these possibilities to some future work.

The authors thank Valerio Bozza, Renkun Kuang, Kento Masuda, Jiyuan Zhang, Keming Zhang and Haimeng Zhao for the discussions and suggestions about the code development. This work is supported by the National Natural Science Foundation of China (grant Nos. 12133005 and 12173021). The authors acknowledge the Tsinghua Astrophysics High-Performance Computing platform at Tsinghua University for providing computational and data storage resources that have contributed to the research results reported within this paper.

Software: Numpy (van der Walt et al. 2011; Harris et al. 2020), Scipy (Virtanen et al. 2020), Matplotlib (Hunter 2007; Droettboom et al. 2016), Jax (Bradbury et al. 2018), VBBinaryLensing (Bozza 2010; Bozza et al. 2018), emcee (Foreman-Mackey et al. 2013), corner (Foreman-Mackey 2016), Numpyro (Bingham et al. 2019; Phan et al. 2019), BlackJax (Cabezas et al. 2024), Jupyter (Kluyver et al. 2016)

REFERENCES

- Aberth, O. 1973, *Mathematics of Computation*, 27, 339, doi: [10.1090/S0025-5718-1973-0329236-7](https://doi.org/10.1090/S0025-5718-1973-0329236-7)
- Akeson, R. L., Chen, X., Ciardi, D., et al. 2013, *PASP*, 125, 989, doi: [10.1086/672273](https://doi.org/10.1086/672273)
- Ansel, J., Yang, E., He, H., et al. 2024, in 29th ACM International Conference on Architectural Support for Programming Languages and Operating Systems, Volume 2 (ASPLOS '24) (ACM), doi: [10.1145/3620665.3640366](https://doi.org/10.1145/3620665.3640366)
- Bachelet, E., Norbury, M., Bozza, V., & Street, R. 2017, *AJ*, 154, 203, doi: [10.3847/1538-3881/aa911c](https://doi.org/10.3847/1538-3881/aa911c)
- Bartolić, F. 2023, Thesis, The University of St Andrews, doi: [10.17630/sta/334](https://doi.org/10.17630/sta/334)
- Bennett, D. P., & Rhie, S. H. 1996, *ApJ*, 472, 660, doi: [10.1086/178096](https://doi.org/10.1086/178096)
- Bezanson, J., Edelman, A., Karpinski, S., & Shah, V. B. 2017, *SIAM Review*, 59, 65, doi: [10.1137/141000671](https://doi.org/10.1137/141000671)
- Bingham, E., Chen, J. P., Jankowiak, M., et al. 2019, *J. Mach. Learn. Res.*, 20, 28:1. <http://jmlr.org/papers/v20/18-403.html>
- Bond, I. A., Abe, F., Dodd, R. J., et al. 2001, *MNRAS*, 327, 868, doi: [10.1046/j.1365-8711.2001.04776.x](https://doi.org/10.1046/j.1365-8711.2001.04776.x)
- Bozza, V. 2010, *MNRAS*, 408, 2188, doi: [10.1111/j.1365-2966.2010.17265.x](https://doi.org/10.1111/j.1365-2966.2010.17265.x)
- Bozza, V., Bachelet, E., Bartolić, F., et al. 2018, *MNRAS*, 479, 5157, doi: [10.1093/mnras/sty1791](https://doi.org/10.1093/mnras/sty1791)
- Bozza, V., Saggese, V., Covone, G., Rota, P., & Zhang, J. 2024, arXiv e-prints, doi: [10.48550/arXiv.2410.13660](https://doi.org/10.48550/arXiv.2410.13660)
- Bradbury, J., Frostig, R., Hawkins, P., et al. 2018, JAX: composable transformations of Python+NumPy programs, 0.3.13. <http://github.com/google/jax>
- Cabezas, A., Corenflos, A., Lao, J., & Louf, R. 2024, BlackJAX: Composable Bayesian inference in JAX. <https://arxiv.org/abs/2402.10797>
- Carpenter, B., Gelman, A., Hoffman, M. D., et al. 2017, *Journal of Statistical Software*, 76, 1, doi: [10.18637/jss.v076.i01](https://doi.org/10.18637/jss.v076.i01)
- Cassan, A. 2017, *MNRAS*, 468, 3993, doi: [10.1093/mnras/stx849](https://doi.org/10.1093/mnras/stx849)
- Crouse, D. F. 2016, *IEEE Transactions on Aerospace and Electronic Systems*, 52, 1679, doi: [10.1109/TAES.2016.140952](https://doi.org/10.1109/TAES.2016.140952)
- Dominik, M. 1998, *A&A*, 333, L79, doi: [10.48550/arXiv.astro-ph/9804059](https://doi.org/10.48550/arXiv.astro-ph/9804059)
- Dominik, M. 2007, *MNRAS*, 377, 1679, doi: [10.1111/j.1365-2966.2007.11728.x](https://doi.org/10.1111/j.1365-2966.2007.11728.x)
- Dong, S., DePoy, D. L., Gaudi, B. S., et al. 2006, *ApJ*, 642, 842, doi: [10.1086/501224](https://doi.org/10.1086/501224)
- Droettboom, M., Hunter, J., Caswell, T. A., et al. 2016, matplotlib: matplotlib v1.5.1, v1.5.1, Zenodo, doi: [10.5281/zenodo.44579](https://doi.org/10.5281/zenodo.44579)

- Duane, S., Kennedy, A. D., Pendleton, B. J., & Roweth, D. 1987, *Physics Letters B*, 195, 216, doi: [10.1016/0370-2693\(87\)91197-X](https://doi.org/10.1016/0370-2693(87)91197-X)
- Eberhard, P., & Bischof, C. 1999, *Mathematics of Computation*, 68, 717, doi: [10.1090/S0025-5718-99-01027-3](https://doi.org/10.1090/S0025-5718-99-01027-3)
- Ehrlich, L. W. 1967, *Commun. ACM*, 10, 107, doi: [10.1145/363067.363115](https://doi.org/10.1145/363067.363115)
- Fatheddin, H., & Sajadian, S. 2022, *MNRAS*, 514, 4379, doi: [10.1093/mnras/stac1565](https://doi.org/10.1093/mnras/stac1565)
- Foreman-Mackey, D. 2016, *The Journal of Open Source Software*, 1, 24, doi: [10.21105/joss.00024](https://doi.org/10.21105/joss.00024)
- Foreman-Mackey, D., Hogg, D. W., Lang, D., & Goodman, J. 2013, *PASP*, 125, 306, doi: [10.1086/670067](https://doi.org/10.1086/670067)
- Gaudi, B. S. 2012, *ARA&A*, 50, 411, doi: [10.1146/annurev-astro-081811-125518](https://doi.org/10.1146/annurev-astro-081811-125518)
- Gaudi, B. S., Bennett, D. P., Udalski, A., et al. 2008, *Science*, 319, 927, doi: [10.1126/science.1151947](https://doi.org/10.1126/science.1151947)
- Geyer, C. 2011, in *Handbook of Markov Chain Monte Carlo*, ed. S. Brooks, A. Gelman, G. Jones, & X.-L. Meng, Vol. 20116022 (Chapman and Hall/CRC), 3–48, doi: [10.1201/b10905-2](https://doi.org/10.1201/b10905-2)
- Gould, A. 2008, *ApJ*, 681, 1593, doi: [10.1086/588601](https://doi.org/10.1086/588601)
- Gould, A., & Gaucherel, C. 1997, *ApJ*, 477, 580, doi: [10.1086/303751](https://doi.org/10.1086/303751)
- Gould, A., & Loeb, A. 1992, *ApJ*, 396, 104, doi: [10.1086/171700](https://doi.org/10.1086/171700)
- Gould, A., Udalski, A., Shin, I. G., et al. 2014, *Science*, 345, 46, doi: [10.1126/science.1251527](https://doi.org/10.1126/science.1251527)
- Harris, C. R., Millman, K. J., van der Walt, S. J., et al. 2020, *Nature*, 585, 357, doi: [10.1038/s41586-020-2649-2](https://doi.org/10.1038/s41586-020-2649-2)
- Hoffman, M. D., & Gelman, A. 2011, arXiv e-prints, doi: [10.48550/arXiv.1111.4246](https://doi.org/10.48550/arXiv.1111.4246)
- Hunter, J. D. 2007, *Computing in Science & Engineering*, 9, 90, doi: [10.1109/MCSE.2007.55](https://doi.org/10.1109/MCSE.2007.55)
- Jonker, R., & Volgenant, T. 1987, *Computing*, 38, 325. <https://api.semanticscholar.org/CorpusID:7806079>
- Kayser, R., Refsdal, S., & Stabell, R. 1986, *A&A*, 166, 36. <https://ui.adsabs.harvard.edu/abs/1986A&A...166...36K>
- Kim, S.-L., Lee, C.-U., Park, B.-G., et al. 2016, *Journal of Korean Astronomical Society*, 49, 37, doi: [10.5303/JKAS.2016.49.1.37](https://doi.org/10.5303/JKAS.2016.49.1.37)
- Kim, Y. H., Chung, S.-J., Yee, J. C., et al. 2021, *AJ*, 162, 17, doi: [10.3847/1538-3881/abf930](https://doi.org/10.3847/1538-3881/abf930)
- Kluyver, T., Ragan-Kelley, B., Pérez, F., et al. 2016, in *Positioning and Power in Academic Publishing: Players, Agents and Agendas*, ed. F. Loizides & B. Schmidt (IOS Press), 87–90. <https://eprints.soton.ac.uk/403913/>
- Lam, C. Y., Lu, J. R., Udalski, A., et al. 2022, *ApJL*, 933, L23, doi: [10.3847/2041-8213/ac7442](https://doi.org/10.3847/2041-8213/ac7442)
- Mao, S., & Paczynski, B. 1991, *ApJ*, 374, L37, doi: [10.1086/186066](https://doi.org/10.1086/186066)
- Margossian, C. C. 2018, arXiv e-prints, arXiv:1811.05031, doi: [10.48550/arXiv.1811.05031](https://doi.org/10.48550/arXiv.1811.05031)
- Milne, E. A. 1921, *MNRAS*, 81, 361, doi: [10.1093/mnras/81.5.361](https://doi.org/10.1093/mnras/81.5.361)
- Mróz, P., Udalski, A., & Gould, A. 2022, *ApJL*, 937, L24, doi: [10.3847/2041-8213/ac90bb](https://doi.org/10.3847/2041-8213/ac90bb)
- Neal, R. 2011, in *Handbook of Markov Chain Monte Carlo*, ed. S. Brooks, A. Gelman, G. Jones, & X.-L. Meng, Vol. 20116022 (Chapman and Hall/CRC), 116–62, doi: [10.1201/b10905-6](https://doi.org/10.1201/b10905-6)
- Pejcha, O., & Heyrovský, D. 2009, *ApJ*, 690, 1772, doi: [10.1088/0004-637X/690/2/1772](https://doi.org/10.1088/0004-637X/690/2/1772)
- Penny, M. T., Gaudi, B. S., Kerins, E., et al. 2019, *ApJS*, 241, 3, doi: [10.3847/1538-4365/aafb69](https://doi.org/10.3847/1538-4365/aafb69)
- Phan, D., Pradhan, N., & Jankowiak, M. 2019, arXiv preprint arXiv:1912.11554
- Poleski, R., & Yee, J. C. 2019, *Astronomy and Computing*, 26, 35, doi: [10.1016/j.ascom.2018.11.001](https://doi.org/10.1016/j.ascom.2018.11.001)
- Sahu, K. C., Anderson, J., Casertano, S., et al. 2022, *ApJ*, 933, 83, doi: [10.3847/1538-4357/ac739e](https://doi.org/10.3847/1538-4357/ac739e)
- Schramm, T., & Kayser, R. 1987, *A&A*, 174, 361. <https://ui.adsabs.harvard.edu/abs/1987A&A...174..361S>
- Skowron, J., & Gould, A. 2012, arXiv e-prints, doi: [10.48550/arXiv.1203.1034](https://doi.org/10.48550/arXiv.1203.1034)
- Udalski, A. 2003, *AcA*, 53, 291, doi: [10.48550/arXiv.astro-ph/0401123](https://doi.org/10.48550/arXiv.astro-ph/0401123)
- van der Walt, S., Colbert, S. C., & Varoquaux, G. 2011, *Computing in Science & Engineering*, 13, 22, doi: [10.1109/MCSE.2011.37](https://doi.org/10.1109/MCSE.2011.37)
- Virtanen, P., Gommers, R., Oliphant, T. E., et al. 2020, *Nature Methods*, 17, 261, doi: [10.1038/s41592-019-0686-2](https://doi.org/10.1038/s41592-019-0686-2)
- Wang, S., Wang, L., & Dong, S. 2025, arXiv e-prints, arXiv:2501.03322. <https://arxiv.org/abs/2501.03322>
- Witt, H. J. 1990, *A&A*, 236, 311. <https://ui.adsabs.harvard.edu/abs/1990A&A...236..311W>
- Witt, H. J., & Mao, S. 1995, *ApJ*, 447, L105, doi: [10.1086/309566](https://doi.org/10.1086/309566)
- Yan, S., & Zhu, W. 2022, *Research in Astronomy and Astrophysics*, 22, 025006, doi: [10.1088/1674-4527/ac3c44](https://doi.org/10.1088/1674-4527/ac3c44)
- Zang, W., Hwang, K.-H., Udalski, A., et al. 2021, *AJ*, 162, 163, doi: [10.3847/1538-3881/ac12d4](https://doi.org/10.3847/1538-3881/ac12d4)
- Zhang, K. 2023, *MNRAS*, 523, 1514, doi: [10.1093/mnras/stad1490](https://doi.org/10.1093/mnras/stad1490)
- Zhang, K., Bloom, J. S., Gaudi, B. S., et al. 2021, *AJ*, 161, 262, doi: [10.3847/1538-3881/abf42e](https://doi.org/10.3847/1538-3881/abf42e)
- Zhao, H., & Zhu, W. 2022, *AJ*, 164, 192, doi: [10.3847/1538-3881/ac9230](https://doi.org/10.3847/1538-3881/ac9230)

Zhu, W., & Dong, S. 2021, *ARA&A*, 59, 291,
doi: [10.1146/annurev-astro-112420-020055](https://doi.org/10.1146/annurev-astro-112420-020055)

Zhu, W., Udalski, A., Gould, A., et al. 2015, *ApJ*, 805, 8,
doi: [10.1088/0004-637X/805/1/8](https://doi.org/10.1088/0004-637X/805/1/8)